The Astrophysical Journal, 631:1180–1190, 2005 October 1

FORMATION AND EVOLUTION OF PLANETARY SYSTEMS: UPPER LIMITS TO THE GAS MASS IN HD 105

D. Hollenbach,[1] U. Gorti,[2] M. Meyer,[3] J. S. Kim,[3] P. Morris,[4] J. Najita,[5] I. Pascucci,[3] J. Carpenter,[6] J. Rodmann,[7] T. Brooke,[6] L. Hillenbrand,[6] E. Mamajek,[8] D. Padgett,[4] D. Soderblom,[9] S. Wolf,[7] and J. Lunine[10]

Received 2005 February 28; accepted 2005 June 9

ABSTRACT

We report infrared spectroscopic observations of HD 105, a nearby (∼40 pc) and relatively young (∼30 Myr) G0 star with excess infrared continuum emission, which has been modeled as arising from an optically thin circumstellar dust disk with an inner hole of size ≳13 AU. We have used the high spectral resolution mode of the Infrared Spectrometer (IRS) on the *Spitzer Space Telescope* to search for gas emission lines from the disk. The observations reported here provide upper limits to the fluxes of H_2 $S(0)$ 28 μm, H_2 $S(1)$ 17 μm, H_2 $S(2)$ 12 μm, [Fe II] 26 μm, [Si II] 35 μm, and [S I] 25 μm infrared emission lines. The H_2 line upper limits place direct constraints on the mass of warm molecular gas in the disk: $M(H_2) < 4.6$, 3.8×10^{-2}, and 3.0×10^{-3} M_J at $T = 50$, 100, and 200 K, respectively. We also compare the line flux upper limits to predictions from detailed thermal/chemical models of various gas distributions in the disk. These comparisons indicate that if the gas distribution has an inner hole with radius $r_{i,\mathrm{gas}}$, the surface density at that inner radius is limited to values ranging from ≲3 g cm^{-2} at $r_{i,\mathrm{gas}} = 0.5$ AU to 0.1 g cm^{-2} at $r_{i,\mathrm{gas}} = 5$–20 AU. These values are considerably below the value for a minimum mass solar nebula, and suggest that less than 1 Jupiter mass (M_J) of gas (at any temperature) exists in the 1–40 AU planet-forming region. Therefore, it is unlikely that there is sufficient gas for gas giant planet formation to occur in HD 105 at this time.

Subject headings: infrared: stars — planetary systems: formation — planets and satellites: formation — solar system: formation — stars: individual (HD 105)

1. INTRODUCTION

Observations of young stars indicate that circumstellar disks of gas and dust are common in the earliest stages of evolution (e.g., Beckwith & Sargent 1996; Hillenbrand et al. 1998; Haisch et al. 2001; Weinberger et al. 2004; Natta et al. 2004). Most of these studies rely on infrared, submillimeter, or millimeter wavelength emission as the signature of small (≲1 mm) warm dust particles, which trace only a small fraction of the circumstellar gas and solid particles. In their initial active accretion phase, circumstellar disks are composed of primordial molecular cloud material, possibly somewhat processed by collapse through the accretion shock onto the disk, with gaseous hydrogen and helium constituting 99% of the total mass and with ∼1% of the disk mass in small dust particles. As infall from the cloud onto the star+disk system diminishes, the gas and dust components of the disk evolve, presumably losing most of the gas via accretion onto the central star or photoevaporation back to the interstellar medium (Hollenbach et al. 1994; Johnstone et al. 1998; Clarke et al. 2001; Adams et al. 2004). Some of the small dust grains presumably coagulate, growing to eventually form planetesimals and rock/ice planets (e.g., Pollack et al. 1996; Weidenschilling 1977; Weidenschilling et al. 1997). During these processes, the circumstellar disk undergoes a transition from being optically thick and (mostly) gaseous to becoming optically thin and (mostly) dusty. There have been many theoretical and observational studies of disks in various stages of evolution that point toward such a sequence (e.g., Weidenschilling et al. 1997; Suttner & Yorke 2001; Throop et al. 2001; Przygodda et al. 2003; Hogerheijde et al. 2003; Testi et al. 2003; van Boekel et al. 2003; Wolf et al. 2003; Dullemond & Dominik 2004; Kessler-Silacci et al. 2005). Such studies have, however, concentrated only on the more readily observed dust emission from the disk, and suggest the evolution of dust to larger particle sizes and hence lower opacity (Miyake & Nakagawa 1993).

Observations of gas and its evolution are in their infancy. Most studies to date have probed either at near-infrared wavelengths (often CO vibrational transitions) the very hot inner surface regions less than ∼1 AU from the star (Carr et al. 2001; Brittain et al. 2003; Najita et al. 2003; Blake & Boogert 2004; Rettig et al. 2004; Thi et al. 2005), or at millimeter wavelengths (often CO rotational transitions) extended gas-rich disks that are hundreds of AU in size (e.g., Skrutskie et al. 1991; Zuckerman et al. 1995; Dutrey et al. 1998; Duvert et al. 2000; Pietu et al. 2003; Qi et al. 2003; Dent et al. 2005; Greaves 2004). The millimeter observations are generally not sensitive to gas at ≲30 AU because the lines become beam-diluted and weak. In addition, the trace species used as millimeter-wavelength probes of gas may freeze out onto grain surfaces at ≳30 AU, making these observations somewhat unreliable for estimating gas masses (e.g., van Dishoeck 2004).

The presence or absence of gas in the planet-forming 1–30 AU regions is difficult to constrain from observations in the near-infrared or millimeter wavelengths. Temperatures in these regions may range from 300 to 50 K; warm gas emitting at these temperatures is best probed in the mid-infrared lines of H_2 at 28.2 and 17.0 μm, and in the mid-infrared fine-structure lines of abundant ions and atoms, such as [S I] 25.2 μm (Gorti & Hollenbach

[1] NASA Ames Research Center, Moffett Field, CA 94035.
[2] University of California, Berkeley, CA 94720.
[3] Steward Observatory, University of Arizona, Tucson, AZ 85721.
[4] *Spitzer* Science Center, California Institute of Technology, Pasadena, CA 91125.
[5] National Optical Astronomy Observatory, Tucson, AZ 85719.
[6] California Institute of Technology, Pasadena, CA 91125.
[7] Max-Planck-Institut für Astronomie, Heidelberg, Germany.
[8] Harvard-Smithsonian Center for Astrophysics, Cambridge, MA 02138.
[9] Space Telescope Science Institute, Baltimore, MD 21218.
[10] Lunar Planetary Laboratory, University of Arizona, Tucson, AZ 85721.

2004, hereafter GH04). These lines are difficult or impossible to observe from the ground. Furthermore, the strong dust continuum of very young objects makes the line-to-continuum ratio quite low, and the background noise high, unless the lines are spectroscopically resolved (requiring resolving powers from 30,000 to 100,000). The *Infrared Space Observatory* (*ISO*) provided some tantalizing evidence for long-lived gas-rich disks by observing mid-infrared emission lines of H_2 toward debris disk candidates (Thi et al. 2001). However, ground-based observations (Richter et al. 2002; Sheret et al. 2003; Sako et al. 2005), *FUSE* results (Lecavalier des Etangs et al. 2001), and *Spitzer* observations (Chen et al. 2004) have called some of these results into question. Recently, ground-based IR and space-based UV observations have detected rovibrational (e.g., Bary et al. 2003) and fluorescent (e.g., Herczeg et al. 2002) H_2 emission toward young disks. The fluorescent H_2 emission is found to occur from warm gas probably located within a few AU of the star. The narrow line widths of the rovibrational IR emission suggest that the emission occurs at much larger distances from the star (>10 AU), and arises either from nonthermal UV pumping or from the X-ray heating of a very small amount of H_2 gas located in the low-density upper atmosphere. The likely nonthermal excitation of the H_2 seen in both the IR and UV makes it difficult to convert the detected line strengths into gas masses.

The nature of gas and dust evolution in circumstellar disks is an intriguing problem for various reasons. A determination of the gas dispersal timescales is important for understanding the formation of planetary systems, and specifically for discriminating between the two competing theories of gas giant planet formation. Core accretion theories of gas giant formation (e.g., Lissauer 1993; Pollack et al. 1996; Kornet et al. 2002; Hubickyj et al. 2004) require long ($\gtrsim$1 Myr) gas disk lifetimes to facilitate the formation of rocky cores of a few Earth masses and subsequent gas accretion to form planets. Detection of gas in older ($\sim 3 \times 10^6$ yr) disks would help validate this scenario. The alternate theory of gravitational instability in disks (e.g., Boss 2003) allows rapid formation of gas giants and dissipation of the gas. The presence of small amounts of gas in the "terrestrial" zone, 0.1–5 AU, in later evolutionary stages ($\sim$10 Myr) influences the dynamics of the smaller planets and planetesimals and is decisive in the final outcome of the planetary system (Agnor & Ward 2002; Kominami & Ida 2002, 2004). Only a narrow range of gas masses ($\sim 0.01 M_J$) in this stage of terrestrial planet formation allow for the formation of an Earth-sized planet in an orbit as circular as the Earth's. At even later stages ($>10^7$ yr) in disk evolution, small masses of gas ($\sim 0.01 M_J$) can affect dust dynamics via drag forces and hence significantly influence disk structure (Klahr & Lin 2001; Takeuchi & Artymowicz 2001; Takeuchi & Lin 2002), thus weakening the interpretation of gaps and ring signatures as being due to the presence of planets.

This paper highlights the potential of the recently launched *Spitzer Space Telescope* to detect small amounts of gas (or to set stringent limits on gas mass) in the planet-forming regions of disks around nearby young stars. *Spitzer* is able to observe the thermal emission from deep layers in the planet-forming zone, sampling significant mass in this 0.3–30 AU intermediate zone that is inaccessible to most other techniques. Gas in these regions is likely to be warm ($\sim$100 K), and line emission at the mid-infrared (10–37 μm) wavelengths seen by the *Spitzer* Infrared Spectrometer (IRS) instrument can probe total gas masses as small as $\sim 0.01 M_J$ in the inner (<20 AU) regions around nearby ($\lesssim$30 pc) stars (GH04). Gas line diagnostics in the *Spitzer* band include the $S(0)$, $S(1)$, and $S(2)$ pure rotational lines of H_2, atomic fine-structure lines of [S I], [Fe I], [Si II], and [Fe II], and molecular lines of OH and H_2O (GH04).

The Formation and Evolution of Planetary Systems (FEPS) *Spitzer* Legacy Science Project (M. Meyer et al. 2005, in preparation) aims to study the evolution of gas in disks by targeting a carefully chosen sample of about 40 nearby solar-type stars for high-resolution ($R \simeq 700$) spectroscopic observations by the IRS (Houck et al. 2004). The sample was selected mainly on the criteria that they span an age range of 3–100 Myr, and that they be nearby (<140 pc), so that the expected weak line fluxes may be detectable with the IRS. A secondary criterion was that they show some infrared excess emission indicative of the presence of dusty disks. To some extent, we favored sources with strong X-ray luminosities, since the X-rays heat the putative gas and intensify the resulting line luminosities. This will be the most comprehensive survey to date of gas in transition and post-accretion systems, aiming to characterize its dissipation and to place limits on the time available for giant planet formation.

In this paper, we present high-resolution IRS data and detailed modeling results for one of the first sources observed through the FEPS gas program, HD 105. HD 105 is a young ($\sim$30 Myr) solar-type star 40 pc from the Sun with an infrared excess indicative of a dust disk (Meyer et al. 2004, hereafter M04). The star has completed its active accretion phase, and the dust continuum is characteristic of an optically thin debris disk. The youth and proximity of the star, the presence of dust (which may imply associated gas), the relatively low dust continuum luminosity, which allows the detection of weak gas lines, and the presence of X-ray flux from the central star (a source of gas heating) make HD 105 a promising candidate for the detection of mid-infrared gas lines. *Spitzer spectroscopic observations of HD 105, however, did not detect any gas emission lines, but instead set stringent upper limits on the line fluxes.* The line flux upper limits are used to set limits on the gas surface density and mass in HD 105. Assuming that the gas distribution has an inner hole of radius $r_{i,\mathrm{gas}}$ greater than about 0.5 AU, we find that there is very little gas in the disk beyond the inner hole, suggesting the end of the main planet-building epoch for gas giants in these regions.

Debris disks have been observed around early (e.g., 49 Cet, A1 V) and late-type (e.g., AU Mic, M1 V) stars and are often characterized by their fractional infrared luminosities, $f = L_{\mathrm{IR}}/L_{\mathrm{bol}}$, which range from 10^{-5} to 10^{-3}. HD 105 is thus a somewhat luminous debris disk, with a fractional infrared luminosity, $f = L_{\mathrm{IR}}/L_{\mathrm{bol}} \sim 4 \times 10^{-4}$. The disk may have evolved past its main planet formation stage, and is young enough to perhaps be a "transition object" with some residual, detectable gas. Although gas is readily detected in young disks (ages of a few Myr, and $f \gtrsim 0.01$, e.g., Dent et al. 2005), most debris disks do not appear to have detectable amounts of gas. Notable exceptions are the disks around 49 Cet ($f \sim 10^{-3}$) and β Pic ($f \sim 10^{-3}$). CO emission has been observed from the $J = 3 \rightarrow 2$ (Dent et al. 2005) and $J = 2 \rightarrow 1$ (Zuckerman et al. 1995) transitions from the disk around 49 Cet, and *ISO* detected H_2 28 μm emission as well (Thi et al. 2001). In β Pic gas emission from metal atoms and ions orbiting in a disk has also been reported, most recently by Brandeker et al. (2004). They and Thebault & Augereau (2005) derive gas masses in the disk of $\sim$0.1–0.4 $M_\oplus$. This amount of gas is insufficient to brake the ions against radiation pressure; both groups estimate $\sim$40 $M_\oplus$ is needed for braking. Chen et al. (2004) obtain upper limits on *warm* gas in β Pic of about 11 $M_\oplus$, although these *Spitzer* observations of the pure rotational lines of H_2 are not sensitive to the presence of cold (<50 K) or atomic gas. The directly detected gas suggests gas depletion in debris disks relative to the dust, in the few instances

where gas has been observed. HD 105 is the first debris disk observed in our FEPS H_2 program, which aims to study gas dispersal in disks as they evolve. As we show below, depending on the gas temperature, *Spitzer* is able to detect gas masses $\gtrsim 1-10\,M_\oplus$ for sources as close as HD 105.

The outline of the paper is as follows. We describe the source in § 2, and discuss the analysis of the *Spitzer* observations in § 3. We then describe the gas and dust disk modeling in § 4. Our results are discussed in § 5, and the summary and conclusions presented in § 6.

2. SOURCE DESCRIPTION

HD 105 is a G0 V spectral type star (Houk 1978) located at a *Hipparcos* distance of 40 ± 1 pc (Perryman et al. 1997). On the basis of its observed space motion and corroborating age diagnostics, Mamajek et al. (2004) conclude that it is a likely member of the Tuc-Hor association. This membership suggests an age of ~30 Myr for HD 105. There are various other indicators of the young age of this dwarf: its Li I λ6707 equivalent width (e.g., Cutispoto et al. 2002) is similar to that of the ~50 Myr old members of the IC 2602 and 2391 clusters (Randich et al. 2001), and is stronger than that of the 120 Myr old Pleiades stars (Soderblom et al. 1990). HD 105 has an active chromosphere, as revealed by the detection of Ca II H and K emission (Henry et al. 1996), and its X-ray luminosity ($L_X = 2.4 \times 10^{29}$ ergs s^{-1}) suggests youth (Metanomski et al. 1998; Wichmann et al. 2003). On the basis of all these indications, we assigned an age of 30 ± 10 Myr for HD 105 (M04).

Early *ISO* observations showed that HD 105 displays infrared excess emission at 60 and 90 μm (Silverstone 2000). Our recent *Spitzer* measurements detect no excess emission at 24 μm, confirm the excess at 70 μm, and detect dust emission even at 160 μm (M04). B. Mazin (2004, private communication) reports a 3 σ upper limit to the 350 μm continuum flux of 2.1 Jy. We have searched the *GALEX* database at the position of HD 105 and found a source offset from the HD 105 position by about 3.″2 in the near-ultraviolet (NUV), but by only 0.″09 in the far-ultraviolet (FUV), whereas the typical positional uncertainty is about 1″. However, there is no other *GALEX* source within 30″ of HD 105. Figure 1 shows the Kurucz model spectral energy distribution (SED) and the observed SED, including the infrared, submillimeter, and *GALEX* data. As expected for a young star, the source has FUV excess. M04) presented early models of the dust distribution implied by the far-infrared excesses. The lack of detectable excess emission at wavelengths shorter than 35 μm implies very little circumstellar dust in the inner (≲15 AU) disk. We discuss these early models and other possible model fits in § 4.

3. OBSERVATIONS AND ANALYSIS

3.1. *Observations and Data Reduction*

We obtained 9.9–37.2 μm spectra of HD 105 on UT 2003 December 14 using the Infrared Spectrograph on *Spitzer* (IRS; Houck et al. 2004; Werner et al. 2004). The spectra we present here were obtained with the two echelle modules ($R = 700$) covering 9.9–19.5 μm with the Short High (SH) detector array, and 18.9–37.2 μm with the Long High (LH) array. We also acquired low-resolution observations ($R = 80$), which were used to account for background flux levels (discussed below). The spectra were acquired using the standard staring mode astronomical observation template (AOT), in which the telescope is nodded to place the star at two positions along each slit, resulting in four separate pointings (two for SH, and two for LH). For the SH observations, we used integration times of 31.5 s for each data collection event (DCE), and cycled eight times for a total on-source exposure time of 504 s. For LH we used the 14.7 s integration time, also cycled eight times, for a total exposure time of 235 s. High-accuracy blue peak-up (13.3−18.7 μm) was performed on the star to ensure a pointing accuracy within 0.″4. The brightness profile of HD 105 in the peak-up image agrees with that expected from the point-spread function.

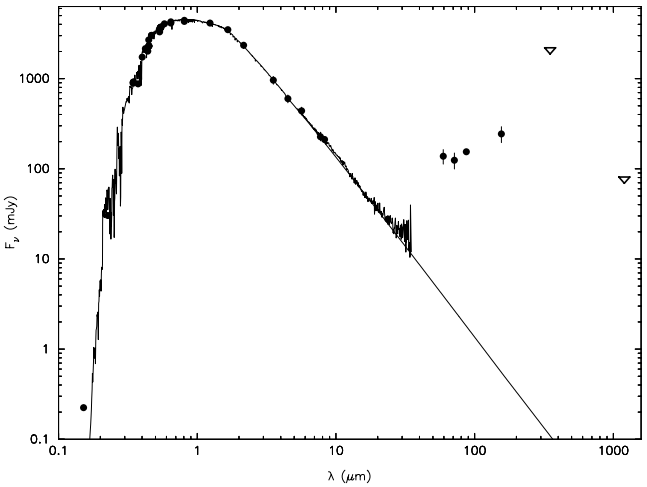

FIG. 1.—Observations and Kurucz model of HD 105. The solid curve through the observed fluxes is the best-fit Kurucz model with $T_{\rm eff} = 6063$ K, $A_V = 0.0$, and $\log g = 4.7$. Also shown are the *ISO* data at 60 and 90 μm (Silverstone 2000), our own *Spitzer* MIPS and low-resolution IRS data (M04), *GALEX* data taken from its archive, a 350 μm upper limit provided by B. Mazin, and a 1 mm upper limit from Carpenter et al. (2005).

Individual DCEs were processed through the *Spitzer* Science Center (SSC) pipeline (ver. S10.5.0), resulting in Basic Calibrated Data (BCD) products to which basic detector calibrations, dark current subtraction, cosmic-ray detection, integration-ramp fitting, and reduction to individual, two-dimensional slope images in units of e s^{-1} pixel^{-1} have been applied. Dark current measurements taken with the LH module within 12 hr of the HD 105 observations were used to mitigate the effects of outlier pixels, whose dark currents vary on timescales of one to several days, rather than using standard dark current subtraction, which employs darks taken over a wider separation in time.

The number of LH outlier pixels (high dark current pixels not representative of expected Gaussian noise) is less than 6% of the 128 × 128 pixels on the array. However, they may dominate the noise within each echelle order if untreated. Corrections were applied to pixels flagged as anomalous in the pipeline due to cosmic-ray saturation early in the integration, or preflagged as unresponsive. For these pixels we applied a cubic spline interpolation technique, relying on 1.5 resolution elements on either side of the dead pixels in the dispersion direction. This signal reconstruction method has been successfully verified with observations of spectral standard stars exhibiting resolved and unresolved emission lines, particularly for the LH array.

Individual one-dimensional spectra were extracted from two-dimensional images flat-fielded with observations of the zodiacal background. We used the off-line SSC software to extract these spectra using the full width of each echelle order. Spectral response and flux calibration corrections were applied to these one-dimensional spectra. The response functions and flux calibration are based on similarly processed and spatially flat-fielded observations of photometric standards HR 6688 (K2 III), HR 6705 (K1.5 III), HR 7310 (G9 III), and HR 2194 (A0 V), and the MARCS code stellar atmosphere models tailored for these

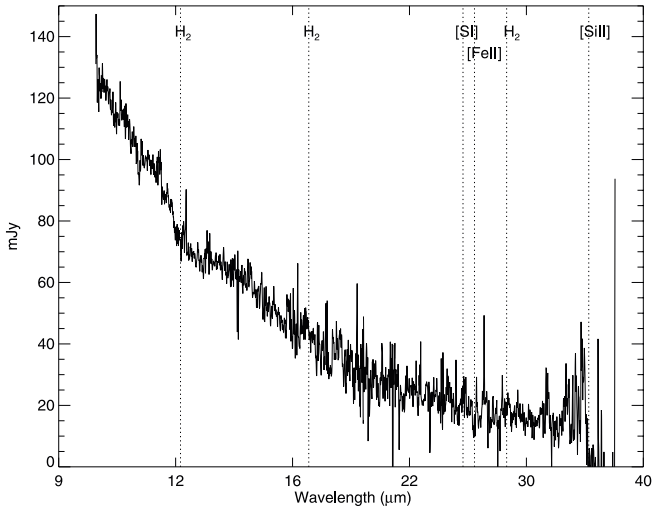

FIG. 2.—IRS spectrum of the 10–38 μm wavelength covered by SH and LH, the high-resolution mode.

stars (Decin et al. 2004). The response correction of the short-wavelength end of the SH data (9.9–12.0 μm) of HD 105 relied solely on HR 2194, in order to minimize any possible discrepancies in the strength of the SiO fundamental band in the K giants.

The 16 individual spectra for each module were next median combined on a spectral order basis. Each order was trimmed, removing $\sim$5% of the data at the blue ends, where the throughput response of the arrays is lowest. The signal-to-noise ratio (S/N) in the continuum is lower than the S/N that would be inferred from repeatability among the 16 spectra. This suggests that the S/N is limited by residual errors due to fringing, uncertainty in the spectra response function, and anomalous pixels, among others. The errors in absolute fluxes, which here include both the star and zodiacal background, are thought to be $\sim$20%.

Although we did not obtain off-source exposures with SH or LH for sky subtraction, we applied approximate corrections based on the background estimator available in the SPOT planning tool. These fluxes are provided in MJy sr^{-1}, which we then converted to Jy using the solid angles subtended by the SH and LH apertures (1.25×10^{-9} sr and 5.82×10^{-9} sr, respectively). Since the SPOT background estimate is derived from measurements made with low spatial resolution, we also compared the extracted sky spectrum obtained with the IRS near HD 105 at low spectral resolution. We found agreement to within 20% with the fluxes provided by the background estimator between 15 and 40 μm when scaled by the appropriate solid angles.

Figure 2 shows the high-resolution spectrum of HD 105. Figure 3 highlights the regions around the strongest emission lines expected from our models (GH04). The S/N is $\sim$12 in the 16–18 μm range, where the noise is computed as the 1 σ rms spread in the ratio between the sky-subtracted IRS spectrum and the adopted Kurucz photospheric model over this essentially featureless region of the continuum [excluding the 16.9–17.1 μm range, where we searched for evidence of the H_2 $S(1)$ line]. Similarly, we estimate a S/N of $\sim$10 in the 26.5–28.5 μm range. The S/N becomes very low at $\lambda > 35$ μm, where the LH throughput is at its lowest.

3.2. *Analysis*

To estimate upper limits of unresolved lines, we fit the spectrum using a Levenberg-Marquardt (LM) algorithm assuming a Gaussian for the line profile and a second-order polynomial for the continuum. The central wavelength of the line was fixed in the fit, as was the width of the Gaussian, to match the instrumental line profile. To fit the baseline locally, we used a wavelength

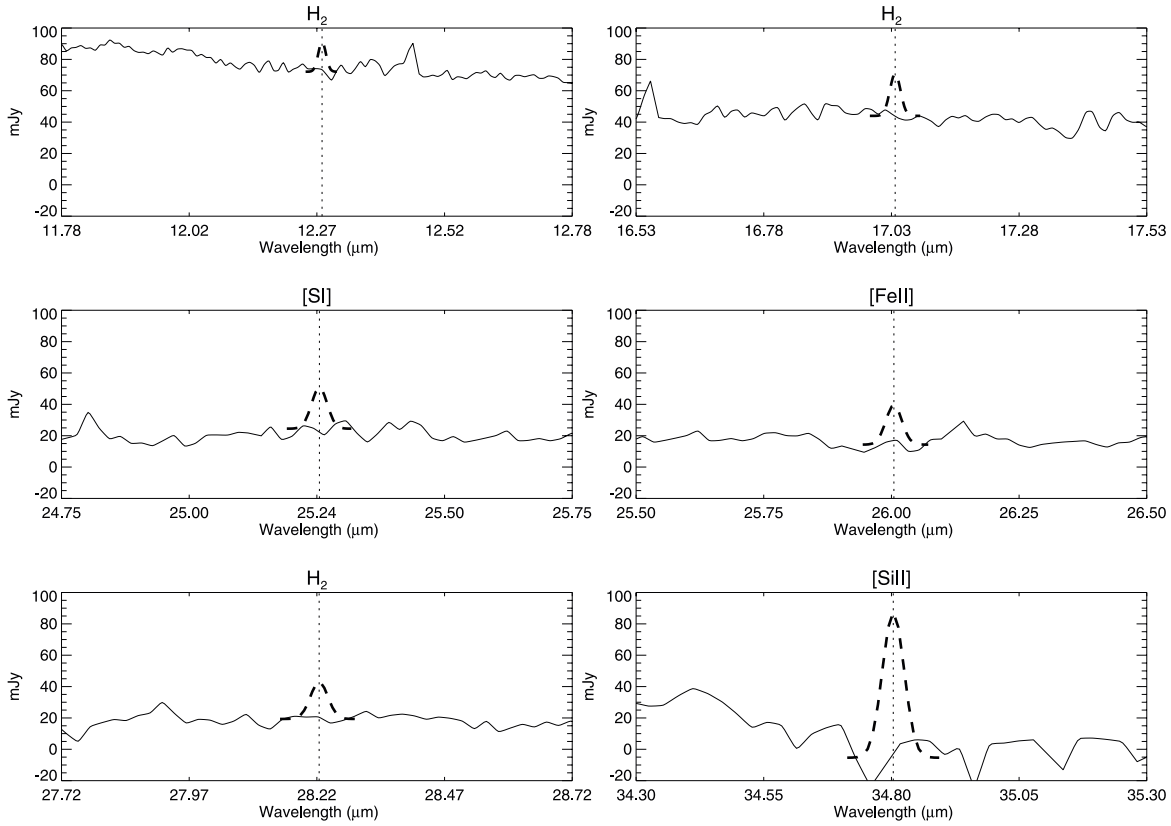

FIG. 3.—Expanded view of the wavelength regions around the expected strong lines. Also shown by dashed lines are the hypothetical 5 σ line fluxes.

TABLE 1
Line Flux Upper Limits Obtained by *Spitzer* IRS High-Resolution Observations of HD 105

Gas Species	Wavelength (μm)	Line Flux Upper Limits (W cm^{-2})
H_2 $S(2)$	12.28	7.1×10^{-22}
H_2 $S(1)$	17.035	7.2×10^{-22}
S I	25.249	4.7×10^{-22}
Fe II	26.000	4.4×10^{-22}
H_2 $S(0)$	28.221	3.8×10^{-22}
Si II	34.800	1.2×10^{-21}

range of ± 0.5 μm centered on each feature (see Table 1). We derived 5 σ upper limits to the line flux for each nondetection by taking the local rms dispersion in the averaged continuum over 2 pixels per resolution element. We show examples of hypothetical 5 σ lines in Figure 3. Several anomalous pixels are evident in the spectra (e.g., at 12.45 and 16.56 μm) that were not flagged in the data reduction discussed in § 3.1. Since these do not correspond to any expected emission lines, this suggests that residual systematic effects may be present in the spectra shown. Table 1 gives the upper limits to the line fluxes of H_2, [S I], [Fe II], and [Si II] lines to estimate upper limits of gas mass in this system.

4. MODELING THE GAS AND DUST IN THE DISK AROUND HD 105

4.1. *Simple Estimate of the Upper Limit to Warm* H_2 *Mass*

Before presenting detailed models of gas/dust disks around HD 105, which can provide estimates of upper limits to the *total* gas mass in atomic and molecular form and at a (model–determined) range of temperatures, we calculate here a simple upper limit to the warm H_2 mass assumed to be at a constant temperature T in the HD 105 disk. We use the upper limits on the H_2 $S(0)$ 28 μm and $S(1)$ 17 μm line fluxes to directly set limits on the mass of warm H_2 at temperature T in HD 105.

The H_2 $S(0)$ and $S(1)$ transitions have critical densities much lower than the gas density in disks with gas masses $\gtrsim 3 \times 10^{-5} M_J$, the extreme lower limit for H_2 line detection by *Spitzer* for HD 105 or other sources at 40 pc (see below). Therefore, for any detectable disk or even for disks with H_2 masses somewhat below detectability, the lower rotational levels (i.e., $J = 0$–3) of H_2 are in LTE.

With LTE and optically thin assumptions, we calculate the mass $M(H_2)$ of molecular gas at temperature T and at the distance (40 pc) of HD 105 that will produce a line flux F for both the $S(0)$ and $S(1)$ transitions,

$$M(\mathrm{H_2}) \simeq 2.8 \times 10^{-5} \left(\frac{F_{S(0)}}{10^{-22}\ \mathrm{W\,cm^{-2}}}\right)\left(1 + \frac{T}{85\ \mathrm{K}}\right) e^{510\ \mathrm{K}/T} M_J, \quad (1)$$

$$M(\mathrm{H_2}) \simeq 7.4 \times 10^{-7} \left(\frac{F_{S(1)}}{10^{-22}\ \mathrm{W\,cm^{-2}}}\right)\left(1 + \frac{T}{85\ \mathrm{K}}\right) e^{1020\ \mathrm{K}/T} M_J. \quad (2)$$

Using these equations and the upper limits for the line fluxes given in Table 1, we find upper limits on the H_2 gas mass of $4.6 M_J$ at 50 K, $3.8 \times 10^{-2} M_J$ at 100 K, and $3.0 \times 10^{-3} M_J$ at 200 K. The $S(0)$ line flux sets the limit at 50 and 100 K, whereas the $S(1)$ line flux sets the limit at 200 K. The $S(2)$ line does not set useful limits at these low temperatures, where it is very weak. Note that assuming long *Spitzer* integrations that set H_2 $S(1)$ flux limits of order $\sim 10^{-22}$ W cm^{-2}, the minimum H_2 mass detectable at 40 pc via the $S(1)$ line is $3 \times 10^{-5} M_J$, achieved when the gas is $T \sim 1020$ K (see eq. [2]). Equations (1) and (2) simply relate the flux in an H_2 line to the mass of gas at a particular temperature. In the following section, we apply much more sophisticated models which actually calculate the temperature distribution in a disk and relate the fluxes to the total mass of gas distributed in the disk.

4.2. *Thermal/Chemical Modeling of Gas and Dust*

4.2.1. *Dust Modeling*

The Spectral Energy Distribution (SED) obtained from existing data in the literature and new *Spitzer* observations (see Fig. 1) has been modeled using the dust disk models of Wolf & Hillenbrand (2003). The initial dust disk model for HD 105 was presented in M04, and we only give a brief description of these previous results here. The observed infrared continuum excess cannot be uniquely fitted by any one particular dust model, but requires a range of dust parameters. M04 assumed for simplicity that the dust is composed of astronomical silicates with a surface density distribution $\Sigma(r) \propto r^0$. The model fits were relatively insensitive to the exponent in the radial density distribution and the outer disk radius $r_{o,\mathrm{dust}}$, since much of the dust emission at wavelengths shorter than the peak emission arises from dust near the inner radius, $r_{i,\mathrm{dust}}$. A grain size distribution of $n(a) \propto a^{-s}$ with $s = 3.5$ was chosen, representative of regions with grain shattering, and providing somewhat better fits to the data than a single grain size. With such a distribution, most of the dust mass is in the largest particles, while the source of the infrared emission derives from grains with a minimum size $a_{\min}$ (which holds over most of the dust area). We define "dust" to be particles with sizes less than $a_{\max} = 1$ mm, and this definition sets the dust mass for a model fit. The three main parameters that determine the fit to the observed SED are then the inner radius $r_{i,\mathrm{dust}}$, the minimum grain size $a_{\min}$, and the dust mass M_{dust}. Roughly speaking, for a given $r_{i,\mathrm{dust}}$ and $a_{\min}$, the dust mass sets the total solid angle subtended by dust grains, and therefore sets the ratio $L_{\mathrm{IR}}/L_{\mathrm{bol}}$ of the dust infrared luminosity to the stellar bolometric luminosity (an observed quantity which then determines the dust mass). M04 found acceptable fits with $r_{i,\mathrm{dust}} = 32$ AU and $a_{\min} = 8$ μm, and with $r_{i,\mathrm{dust}} = 45$ AU and $a_{\min} = 5$ μm. These best-fit $r_{i,\mathrm{dust}}$ and $a_{\min}$ corresponded to dust masses of 9×10^{-8} and 4×10^{-7} $M_\odot$, respectively.

Since the results presented in M04, we have performed a more extensive parameter study of the best χ^2 fit, and have found that the minimum in χ^2 corresponds to even larger $a_{\min} = 21$ μm and lower $r_{i,\mathrm{dust}} = 19$ AU than explored in M04, and to a somewhat lower dust mass $\sim 7.5 \times 10^{-8}$ $M_\odot$. We found that quite good fits could be obtained for 13 AU $< r_{i,\mathrm{dust}} \lesssim 45$ AU. The inner dust radius cannot be smaller than 13 AU, because the dust becomes too hot and produces excess emission at $\lambda \lesssim 35$ μm. We do not emphasize this SED fitting procedure here because we have found, and show below, that for all acceptable dust models, there is too little dust surface area to affect the gas chemistry, heating, or cooling. Therefore, the gas spectrum is independent of the dust in the case of HD 105, and mainly depends on $r_{i,\mathrm{gas}}$ and the gas surface density Σ_0 at $r_{i,\mathrm{gas}}$, as we discuss below.

4.2.2. *Gas/Dust Disk Models*

We apply the thermal/chemical disk models of GH04 to study HD 105. In these models, a central star and the interstellar radiation field illuminate a gas and (optically thin) dust disk extending

from r_i to r_o. The gas and dust are heated by the radiation field (the gas is particularly sensitive to the UV and X-ray radiation), and the gas and dust temperatures are calculated in separate thermal balance equations. The vertical density structure and chemistry are self-consistently computed by imposing thermal balance, steady-state chemistry, and pressure equilibrium. The assumption is that in the dusty regions the gas and small dust particles are well mixed, so that their density ratio does not vary vertically (no settling of small dust particles). However, as we shall show, there is so little dust in HD 105 that the gas emission lines do not depend on the dust vertical (or radial) distribution. We consider various gas-heating sources, such as gas-dust collisions, X-rays, stellar and interstellar FUV radiation, and exothermic chemical reactions. The cooling is mainly through molecular rotational and atomic and ionic fine-structure emission. In summary, the inputs to the model include the stellar parameters, the interstellar field, r_i and r_o, the surface density distribution of the gas, the dust size distribution, and the dust-to-gas mass ratio (which often is held fixed). Our main input variable is generally the gas surface density distribution. The outputs are the vertical density, chemistry, and temperature distribution as a function of r, and the resulting line intensities of various ionic, atomic, and molecular species. In turn, these line intensities can be compared with line observations to constrain the physical parameters in the disk, such as the gas surface density distribution (or in this case, provide upper limits to gas surface densities).

We first consider a standard case, our best-fit dust distribution discussed in § 4.2.1, with $r_{i,\mathrm{gas}} = r_{i,\mathrm{dust}} = 19$ AU, i.e., *gas and dust coexist spatially*. However, we have found that in this standard case, and in other SED-fitting cases we have tested with coexisting dust where $r_{i,\mathrm{dust}} = 13$–45 AU, the dust has no effect on the gas properties. There is too little surface area to appreciably affect the cooling (through gas-dust collisions), the heating (through the grain photoelectric mechanism), or the H_2 chemistry (through catalysis of H_2 on grain surfaces). Therefore, we have also considered a number of other models with different $r_{i,\mathrm{gas}}$, but we have not included dust since its effect is minimal.

As we show in § 5, the line fluxes from the gas originate from the inner regions, $r_{i,\mathrm{gas}} < r < r_{w,\mathrm{gas}}$, where $r_{w,\mathrm{gas}}$ is defined such that 90% of the line luminosity is generated from $r_{i,\mathrm{gas}}$ to $r_{w,\mathrm{gas}}$. Considerable (gas) opacity to the stellar photons occurs at $r_{i,\mathrm{gas}}$, so that $r_{w,\mathrm{gas}}$ is typically only slightly ($\sim$10%) larger than $r_{i,\mathrm{gas}}$, leaving the shielded outer gas beyond $r_{w,\mathrm{gas}}$ cold and unemissive. Therefore, there can be very large amounts of cold gas in these outer regions, depending on the gas outer radius. The small amount of emission from this cold gas is below *Spitzer* line flux constraints. The IRS on *Spitzer*, however, is very sensitive to the warm gas just between $r_{i,\mathrm{gas}}$ and $r_{w,\mathrm{gas}}$. Because the emitting region has such a small radial extent, we assume that the gas surface density $\Sigma_{\mathrm{gas}}(r) = \Sigma_0$ is a constant, independent of r in the emitting region. We then vary Σ_0 and compute the line fluxes. The observed line flux limits are then used to constrain Σ_0 and the gas mass M_w between $r_{i,\mathrm{gas}}$ and $r_{w,\mathrm{gas}}$.

If the gas extends far beyond $r_{w,\mathrm{gas}}$, the total mass of the gas in the disk can be estimated from

$$M_{\mathrm{gas}} = \frac{2\pi\Sigma_0 r_{i,\mathrm{gas}}^2}{2-\alpha}\left[\left(\frac{r_{o,\mathrm{gas}}}{r_{i,\mathrm{gas}}}\right)^{2-\alpha} - 1\right] \quad \text{for } \alpha < 2, \quad (3)$$

where the gas surface density is given by $\Sigma_{\mathrm{gas}}(r) = \Sigma_0(r_{i,\mathrm{gas}}/r)^{\alpha}$ for $r_{i,\mathrm{gas}} < r < r_{o,\mathrm{gas}}$. Generally, α is assumed to be $\sim$0–1.5. Note that for $\alpha < 2$ and $r_{o,\mathrm{gas}} \gg r_{i,\mathrm{gas}}$, considerable cold (hidden) gas mass is located at the outer radius $r_{o,\mathrm{gas}}$.

The gas emission line fluxes then depend on only two main parameters, $r_{i,\mathrm{gas}}$ and Σ_0, in the case of HD 105, where dust does not affect the gas properties. The line fluxes vary with these parameters for the following reasons. X-rays and UV photons tend to penetrate and heat a fixed column of gas. Therefore, larger inner holes increase the mass of gas relative to the total disk mass that is affected by X-ray and UV photons. However, at the same time, the stellar radiation flux decreases as $1/r^2$, and the flux incident on the inner edge of the disk decreases as $r_{i,\mathrm{gas}}$ increases. The total energy intercepted by the disk does not vary appreciably with changing $r_{i,\mathrm{gas}}$, because the scale height tends to scale as r, so that the gas disk subtends a fairly constant solid angle. However, the declining flux means a drop in the gas temperature (for fixed density), and the relative strengths of emission lines change. Similarly, Σ_0 controls the gas density at $r_{i,\mathrm{gas}}$, and increasing Σ_0 changes the gas temperature and the relative strengths of the lines. We note that at small enough $r_{i,\mathrm{gas}}$ the lines will become undetectable by *Spitzer* regardless of Σ_0, since the mass and surface area of the emitting gas decline with $r_{i,\mathrm{gas}}$. Optically thin LTE line luminosities are proportional to mass, while optically thick lines are proportional to the emitting area. At very small $r_{i,\mathrm{gas}}$ and when Σ_0 is raised to extremely high values, the lines cannot exceed their (optically thick) blackbody limits, the temperature is finite, and the small surface area and mass drive the beam diluted fluxes below detectability.

We next consider a range of $r_{i,\mathrm{gas}}$ from 0.5 to 100 AU. We have chosen cases of 13, 19, and 45 AU because they correspond to the minimum, the best fit, and an approximation of the maximum $r_{i,\mathrm{dust}}$ allowable from the SED modeling. However, we also consider the possibility that the gas does not coexist with the dust. In each case, we vary Σ_0 and determine the variation in the line fluxes with Σ_0 at the specified inner radius.

5. RESULTS AND DISCUSSION

5.1. *Gas Disks with Inner Holes*

We first discuss the results of the standard case in which we have included the best-fit dust population and $r_{i,\mathrm{gas}} = r_{i,\mathrm{dust}} = 19$ AU. Figure 4 shows that model line luminosities initially increase as the gas mass surface density increases at the inner radius. The flux from the [Si II] line is the strongest, followed by the [S I], [Fe II], and the H_2 $S(1)$ lines. The [Si II] and [S I] lines are seen to plateau at high surface densities as they reach their optically thick blackbody limits and as Si^+ begins to recombine at high density. The dotted lines in Figure 4 show the corresponding *Spitzer* upper limits presented in Table 1. The intersection of the upper limits (*dotted line*) with the model curves (*solid line*) for a given species marks the critical column density $\Sigma_{0,\mathrm{crit}}$ above which the line should have been detected. With this particular choice of $r_{i,\mathrm{gas}}$, the line providing the strongest constraint is the [S I] line, which gives $\Sigma_{0,\mathrm{crit}} \simeq 0.14$ g cm^{-2}.

It is instructive to look at the details of a fiducial model (the standard case at the critical surface density for that case, $\Sigma_{0,\mathrm{crit}} = 0.14$ g cm^{-2}) to understand the typical chemistry, temperature structure, and heating and cooling agents. The upper left panel of Figure 5 shows the gas temperature and temperature of the smallest ($a_{\min} = 21$ μm) dust grains at the midplane as a function of r. The gas density at $r_{i,\mathrm{gas}}$ in the midplane is about 10^9 cm^{-3}. We have suppressed the data from 19 to 19.04 AU (a region where the gas goes from predominantly atomic hydrogen to mostly molecular hydrogen and where soft $\sim$0.5 keV X-rays are absorbed), because of complicated behavior there, which cannot be discerned at this graphic resolution. This small region does not significantly contribute to the line spectrum, since most of the

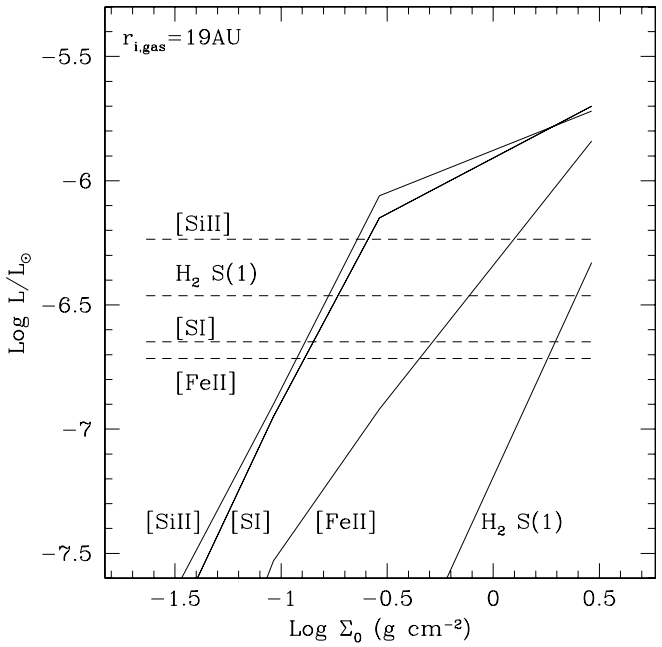

FIG. 4.—Calculated line luminosities (*solid lines*) as a function of gas surface density at the inner radius ($r_{i,\mathrm{gas}} = r_{i,\mathrm{dust}} = 19$ AU) for the strongest lines obtained for the standard model disk with the best-fitting dust to the SED. The dashed lines show observed upper limits on the line luminosities as presented in this paper. Where the dashed lines meet the solid lines for a given transition marks the upper limit to the gas surface density $\Sigma_{0,\mathrm{crit}}$ in the disk as constrained by that transition. In this case, [S I] sets the tightest constraint of $\Sigma_{0,\mathrm{crit}} = 0.14$ g cm^{-2}.

emission arises from the much greater mass of gas that lies between 19.04 and 22 AU. At the inner disk edge (19 AU, not shown), the gas is atomic and fairly warm (∼500 K), but it very quickly cools to about 150 K at 19.04 AU because of the rapid rise in abundance of cooling molecular species such as CO. One sees that beyond 19.04 AU the temperature drops from ∼150 K to about 70 K at 22 AU. The chemistry changes slowly in this region. The hydrogen is mostly H_2, formed by the reaction of H with H^- and on grain surfaces. We have found that eliminating grains does not change the H_2 abundance appreciably (it is nearly entirely molecular in any case). The atomic H abundance is quite high because of the inefficiency of the H^- and grain processes. Most of the sulfur is atomic, and most of the silicon and iron is singly ionized. The carbon is mostly in CO, and all remaining gas-phase oxygen is in atomic O. Note that when $r = 19.1$ AU, there is already a column $N \sim 10^{22}$ cm^{-2} of hydrogen between the central star and that point. Because the densities are very high, and the UV field low, there is considerable H_2, C, CO, S, Si, and Fe in the surface regions, and their column provides considerable opacity to the stellar UV photons via photoionization and photodissociation processes. The dust surface area per hydrogen atom is small, so that dust extinction is not important, and the opacity is entirely due to gaseous species. Similarly, the grain surface area is too small to effectively heat the gas by the grain photoelectric heating mechanism, or to heat or cool the gas by gas-grain collisions. The gas-grain cooling could not be shown in the lower right panel of Figure 5 because it is many orders of magnitude below the graph. We have also run alternate SED-fitting models of allowable $r_{i,\mathrm{dust}}$ and found that dust is not important in HD 105 for modeling the gas in the disk because of its low abundance and surface area.

The main heating mechanisms for the gas in the emission zone are heating by gaseous absorption of X-rays from the central star and stellar optical and UV photons, which photoionize and photodissociate atoms, ions, and molecules. The lower energy X-ray photons are absorbed nearest to the surface and, because of their higher cross sections for absorption, lead to the highest X-ray heating there. The more energetic X-rays penetrate farther, and provide gas heating at greater depths. In the bulk of the emissive zone, the heating by optical and UV photons is dominated by the photoionization of S (which provides most of the electrons) and the photodetachment of electrons from H^-. Note that this latter process requires only stellar optical photons and not the higher energy UV photons. However, this process requires H^-; the H^- is produced by electrons that arise from the photoionization of S and Si, and these photoionizations do require UV photons. The cooling is mainly by CO mid-J rotational transitions (∼200–400 μm), [S I] 25 μm, and [O I] 63 μm. Beyond 22 AU, the cooling is dominated by CO mid-J transitions, as the gas cools below 70 K. If the gas disk extends much beyond 30 AU, these CO transitions become detectable if the CO does not freeze onto the cold grain surfaces. To date, no CO observations of HD 105 have been made. We note that the cooling by CO and [O I] occurs at longer wavelengths ($\lambda > 38$ μm) than accessible by the IRS on *Spitzer*, but these transitions may be detectable by instruments on the future Stratospheric Observatory for Infrared Astronomy (SOFIA) and by the *Herschel Space Observatory*.

Direct heating of the gas by absorption of stellar photons heats the gas to $T \gtrsim 70$ K in the inner regions (19–22 AU) of the gas disk. The gas vertical scale height is proportional to $T^{1/2}$, and the warm gas intercepts about 20% of the stellar radiation due to its flared nature. In many wavelength bands the gas opacity is significant. Therefore, there is significant heating by this mechanism, but it tends to occur at the inner rim ($r_{i,\mathrm{gas}}$), where the stellar fluxes are highest and least attenuated by the gas. The heating at the inner rim makes it expand vertically, enhancing its ability to intercept photons and to shield the outer disk. Dullemond et al. (2001) have discussed this effect for dusty disks in which the opacity is created by dust particles. We find that in the fiducial case, the heated region extends radially about 3 AU beyond $r_{i,\mathrm{gas}}$ to $r_{w,\mathrm{gas}} \simeq 22$ AU. On the order of 90% of the luminosity of the infrared lines studied here are emitted in this narrow annulus. Because of this fact, the gas spectra from the model disks around HD 105, where dust plays no factor, depend only on $r_{i,\mathrm{gas}}$ and the gas surface density Σ_0, as discussed above.

We now present the results of an identical search of Σ_0 parameter space for a variety of $r_{i,\mathrm{gas}}$ from 0.5 to 100 AU, assuming that dust is unimportant. Table 2 lists the surface density limits $\Sigma_{0,\mathrm{crit}}$ as determined from each line. Associated with each of these lines and $\Sigma_{0,\mathrm{crit}}$ are particular values for r_w and M_w, the mass of the warm gas between $r_{i,\mathrm{gas}}$ and r_w. These are also listed in Table 2 for the most sensitive line. Note that the warm gas masses are somewhat less than the simple analytic expression given in § 4.1 for H_2 lines produced in $T \sim 100$ K gas. *Spitzer* can detect masses somewhat smaller than $10^{-2} M_J$ in HD 105 [the limit derived from H_2 $S(1)$ for $T \sim 100$ K gas], because other lines such as [S I] are predicted to be stronger, and, in the cases of small $r_{i,\mathrm{gas}}$, the gas is warmer than 100 K.

The total mass of gas (warm and cold) in any given model depends on the power law of the gas surface density distribution α and on the outermost extent $r_{o,\mathrm{gas}}$ of the gas. Let us assume that the region of gas giant formation extends to about 40 AU, based on the solar system example. We take one of the more extreme values of the power law of the gas surface density distribution, $\alpha = 0$, which maximizes the gas mass in the outer shielded zones. The upper limit (derived from the most sensitive line [S I]) to the total gas mass in this extreme case of low α is then about $1.9 M_J$ for $r_{i,\mathrm{gas}} = 0.5$ AU, $0.2 M_J$ for $r_{i,\mathrm{gas}} = 1$ AU, and $0.1 M_J$ for

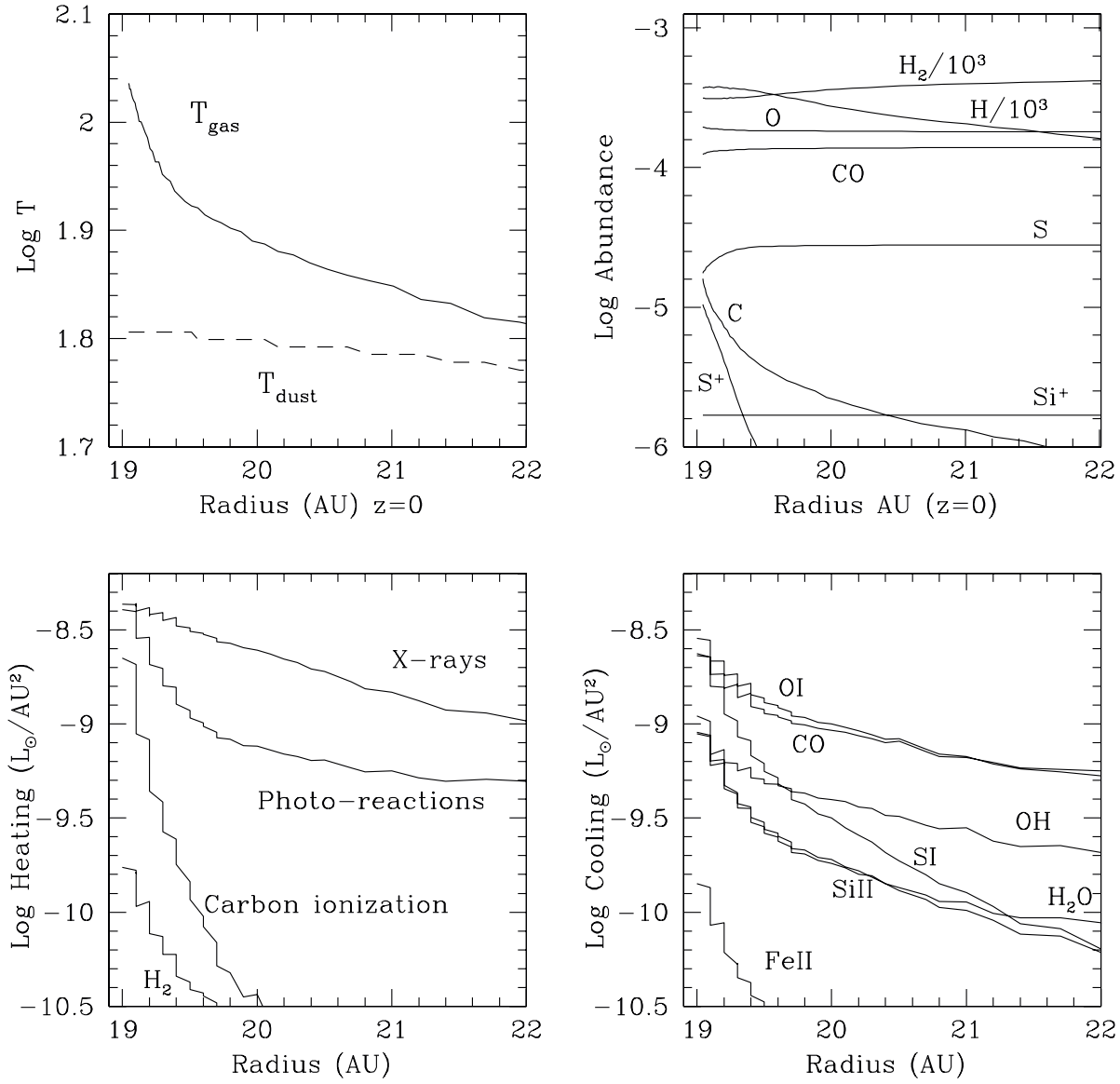

FIG. 5.—Midplane gas and $a_{\min}$ dust temperature, the midplane abundances of the abundant coolants, the total vertically integrated disk heating, and total vertically integrated disk cooling for each species as a function of radius for the emission region extending from $r_{i,\mathrm{gas}} = 19$ AU to somewhat beyond $r_{w,\mathrm{gas}}$. We have suppressed the data from 19 to 19.04 AU for clarity, as discussed in the text.

$r_{i,\mathrm{gas}} = 5$–20 AU, where we basically extrapolate the upper limit on the gas surface density measured at $r_{i,\mathrm{gas}}$ to 40 AU. *Therefore, for* $r_{i,\mathrm{gas}} \gtrsim 0.5$ AU*, there is insufficient gas in HD 105 at this time to feed the formation of gas giants*.

Table 2 shows that the upper limits to the gas surface density at $r_{i,\mathrm{gas}}$ are not very sensitive to $r_{i,\mathrm{gas}}$ for 1 AU $\lesssim r_{i,\mathrm{gas}} \lesssim$ 40 AU. Larger $r_{i,\mathrm{gas}}$ tends to produce more mass of gas heated by the stellar photons, but, because of the dilution of the stellar flux, also tends to lead to lower characteristic gas temperature. These effects counterbalance each other to some extent, resulting in similar line fluxes.

However, for $r_{i,\mathrm{gas}} < 1$ AU, $\Sigma_{0,\mathrm{crit}}$ rises steeply. The heating mechanisms only penetrate to a relatively constant column of $N_w \sim 10^{22}$ cm^{-2}, so the mass of heated gas scales roughly as

TABLE 2

M_w, $r_{w,\mathrm{gas}}$, AND $\Sigma_{0,\mathrm{crit}}$ DERIVED FROM THE OBSERVATIONS AND MODELS

PARAMETER	VALUE AT $r_{i,\mathrm{gas}}$ (AU) =						
	0.5	1.0	5.0	13.0	19.0	45.0	100.0
r_w (AU)	0.69	1.28	5.15	16.5	21.9	48.6	123.0
$\Sigma_{0,\mathrm{crit}}$ (g cm^{-2}) H_2 $S(1)$	...	...	251.10	2.30	1.82	6.39	2.98
$\Sigma_{0,\mathrm{crit}}$ (g cm^{-2}) [Fe II]	6.12	2.32	0.92	0.45	0.45	0.42	1.31
$\Sigma_{0,\mathrm{crit}}$ (g cm^{-2}) [S I]	3.43	0.36	0.12	0.11	0.14	0.21	1.04
$\Sigma_{0,\mathrm{crit}}$ (g cm^{-2}) [Si II]	121.30	21.4	9.35	0.26	0.23	0.41	2.02
log M_w (M_J)	−3.57	−4.09	−4.19	−2.41	−2.22	−1.61	0.6

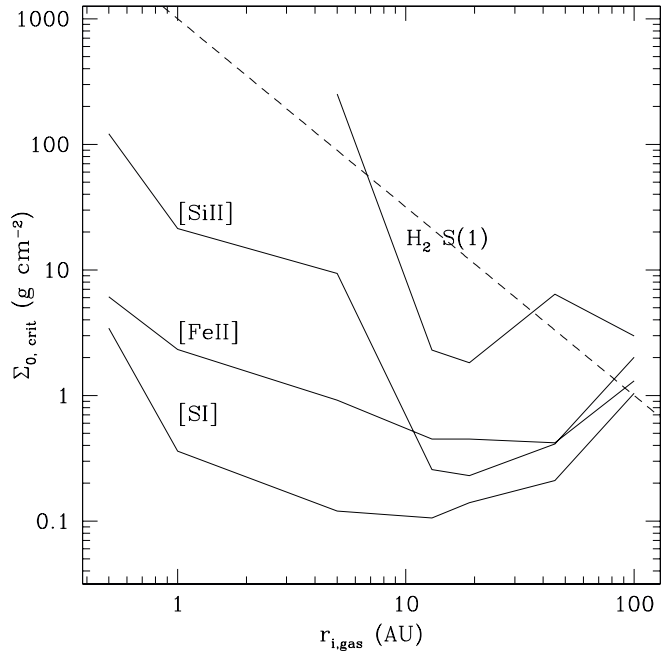

FIG. 6.—Detectable surface density based on *Spitzer* observations of HD 105 for a gas disk with various inner radii, and with the small amount of dust implied by the infrared continuum SED. For small $r_{i,\mathrm{gas}} \lesssim 1$ AU, the lines set poor or no limits, as the warm emissive gas gets too optically thick and beam-diluted to be detectable by *Spitzer*, regardless of the magnitude of Σ_0 (see text). Also shown for comparison is the surface density distribution of the minimum mass solar nebula with radius, $\Sigma(r) = 1000 r_{\mathrm{AU}}^{-3/2}$ g cm^{-2} (*dashed line*).

$r_{i,\mathrm{gas}}^2$, assuming that the vertical scale height scales with radius. Therefore, the mass (or area for optically thick lines) of heated gas decreases as we move inward, and so the gas temperature must rise appreciably in order for the gas to be detected. Since the gas temperature tends to rise with increasing density, due to the collisional de-excitation of the upper levels of cooling transitions, we require substantially more surface density to raise the temperature sufficiently to overcome the loss of warm gas mass and area.

Figure 6 visually shows how the critical surface density $\Sigma_{0,\mathrm{crit}}$ depends on $r_{i,\mathrm{gas}}$. We see that [S I] 25 μm is the most sensitive *Spitzer* line for constraining the gas surface density in gas disks with little dust, like HD 105.

If $r_{i,\mathrm{gas}}$ is sufficiently small ($\lesssim$0.5 AU), the gas mass in the disk is essentially unconstrained by the *Spitzer* observations, because a very small mass and surface area of inner gas shields the outer regions, leaving them too cold to be detected at this time. Clearly, if a line detection is made by *Spitzer* IRS, knowledge of the parameter $r_{i,\mathrm{gas}}$ would be extremely helpful if the line flux is to be converted into $\Sigma_{0,\mathrm{crit}}$ and M_w. Therefore, follow-up observations by higher spectral resolution instruments will be very useful, since resolved line widths can be translated into Keplerian velocities, and hence $r_{i,\mathrm{gas}}$.

5.2. *Discussion*

Assuming that $r_{i,\mathrm{gas}} \gtrsim 0.5$ AU, the *Spitzer* upper limits to the gas lines fluxes in [S I] 25 μm, [Si II] 35 μm, [Fe II] 26 μm, and H_2 $S(1)$ 17 μm provide upper limits to the gas surface density at $r_{i,\mathrm{gas}}$ that would indicate that less than a Jupiter mass of gas is present in the gas giant planet-forming zone extending to 40 AU. It is interesting that the most sensitive indicators of gas are not the H_2 lines, but fine-structure lines (in particular [S I] 25 μm) of less abundant species (see GH04). These upper limits indicate that in this region of possible gas giant planet formation, either a giant planet has already formed or it never will: *the era of significant gas accretion onto protoplanets is over for this 30 Myr old system*.

The main caveat is that if the gas surface density distribution, unlike the dust, extends to the innermost regions ($r_{i,\mathrm{gas}} < 0.5$ AU) of the disk, then significant (i.e., $>1 M_{\mathrm{J}}$) amounts of cold gas could be hidden in the 5–40 AU region where gas giant planets may still be accreting, without violating our observational constraints on the line luminosities. However, if the gas indeed extends to <0.5 AU, then the gas is likely accreting onto the stellar surface. If M_d is the mass of gas from the stellar surface to 40 AU, then the accretion rate onto the central star is given by $\dot{M} \simeq 3 \times 10^{-9} (\alpha/0.01)(M_d/M_{\mathrm{J}})\, M_\odot$ yr^{-1}, where α is the standard alpha viscosity parameter. Such high accretion rates would produce diagnostics such as large UV or near-IR excesses, Hα emission lines, or other indicators of accretion-driven winds, which are not observed. Therefore, we regard this possibility as unlikely.

The gas limits in the 10–40 AU region may also be relevant to theories of the formation of the outer giants such as Neptune and Uranus. A generic problem for these systems is that they dynamically heat (i.e., induce high random velocities in) the much smaller objects that provide potential coalescent collisions that enable them to grow. The higher velocities reduce the gravitational focusing, and therefore reduce their growth rate (Levison & Stewart 2001). Without some kind of dynamical cooling mechanisms, it is difficult for them to form in situ within the lifetime of the solar system. Gas drag is one possibility, but it requires many Jupiter masses of gas. Our upper limits on the amount of gas indicate that, after 30 Myr in HD 105, there is not nearly enough gas drag to have an appreciable effect at this time (see, e.g., Goldreich et al. 2004).

Takeuchi & Artymowicz (2001), Klahr & Lin (2001), and Takeuchi & Lin (2002) showed that a small amount of gas (and the effect of stellar photons on the gas and dust) can sculpt the dust morphology and create an inner hole. Therefore, the sharp inner dust hole at ~19 AU in HD 105 need not reflect the presence of giant planets, but may be produced in a planetless gas/dust disk around HD 105. These authors show that $M_{\mathrm{gas}} > 1-10 M_{\mathrm{dust}}$ produces such effects, and that when $M_{\mathrm{gas}} > 100 M_{\mathrm{dust}}$ the dust grains cannot migrate effectively relative to the gas. Using our upper limits for the case in which the gas and dust are cospatial, we find that we can only constrain the ratio of gas mass to dust mass in HD 105 to values of <1000, and therefore we cannot effectively constrain the effects of gas on the dust dynamics. In other words, the sharp inner rim of dust implied by the IR continuum SED of HD 105 could be produced by a small amount of gas below our upper limits. An alternate hypothesis is that in the absence of gas, a giant planet is preventing dust from the outer debris disk from reaching the inner part of the system, as discussed in M04.

Kominami & Ida (2002, 2004) and Agnor & Ward (2002) discuss the effects of a small amount of gas in the terrestrial zone (1–5 AU) on the resulting formation of terrestrial planets. If $M_{\mathrm{gas}} \gg 10^{-2} M_{\mathrm{J}}$ in the terrestrial zone for tens of millions of years, then lunar and Mars-sized planetary embryos feel the dynamical friction of the gas, circularize their orbits, and never collide to form Earth-mass planets. On the other hand, if $M_{\mathrm{gas}} \ll 10^{-2} M_{\mathrm{J}}$, then the embryos are on eccentric orbits, and collide to form Earth-sized or larger orbits, but with eccentricities substantially larger than the Earth. The suggestion is that the Earth may have formed with roughly $10^{-2} M_{\mathrm{J}}$ of gas in the terrestrial zone for tens of millions of years. The terrestrial zone (~0.3–3 AU) in HD 105 is inside $r_{i,\mathrm{dust}}$ and is currently quite dust-free. Our models show that if the gas extends all the way in to $r_{i,\mathrm{gas}} <$ 0.5 AU, then we are not sensitive to gas mass in the terrestrial

zone, and therefore cannot set useful limits on this process. If for some reason the gas has an inner radius of 0.5–1 AU, we can set limits of about 2×10^{-2} to $2 \times 10^{-3} M_J$ for the mass of gas from this inner radius to 5 AU. In this case, the limits are close to the critical value of $10^{-2} M_J$, and indicate perhaps insufficient gas to prevent large, Earth-sized planets from forming. *Spitzer* may be able to set even more stringent limits on this process in other sources. If sufficient small dust is mixed with the gas in the terrestrial zone, then the gas in the models is hotter, and smaller gas masses can be detected.

Finally, are these upper limits surprising in the context of theoretical calculations that have been performed on the likely dispersal mechanisms of the gas? The current kinematic evidence suggests that HD 105 formed in a small group of tens of stars (see § 2), which likely lacked O or early B-type stars. Assuming that HD 105 was not exposed to high UV fluxes from nearby massive stars, the main dispersal mechanism for the outer disk would likely be photoevaporation of the gas by the central star, and for the inner disk, viscous accretion and spreading of the gas would dominate (Hollenbach et al. 2000; Clarke et al. 2001; Matsuyama et al. 2003). Unfortunately, it is difficult to answer this question because of the lack of self consistent photoevaporation models that treat not just the extreme-UV (EUV; i.e., $h\nu > 13.6$ eV) photons (see Hollenbach et al. 1994), but also the less energetic stellar photons, as well as the X-rays from the young central star. U. Gorti & D. Hollenbach (2005, in preparation) are developing such models, and their preliminary results show that the less energetic photons rapidly (in less than 10 Myr) disperse the gas outside of about 30–50 AU. The EUV photons can potentially remove gas outside of about 1–5 AU, but the evolution of the EUV luminosity and the radiative transfer of these photons as they try to penetrate the protostellar winds in the early stages of star formation are not well determined. A recent paper by Alexander et al. (2005) suggests rather high escaping EUV luminosities, which may rapidly (<10 Myr) remove the outer gas. Once the outer disk is removed, viscosity removes the inner gas on timescales of roughly 0.1 Myr $(0.01/\alpha_v)(r/10\ \mathrm{AU})$, where α_v is the turbulent viscosity parameter in the standard "α" disks.

The value of α_v is typically 10^{-2} if the Balbus & Hawley (1991) magnetorotational instability, or MRI, is operant. The MRI instability requires a minimal level of ionization, which all our relatively low-mass models meet. Assuming that MRI is active, the viscous timescales inside the photoevaporation region (which lies at >3–30 AU) are of the order of 0.03–0.3 Myr—extremely short. On the other hand, it is not totally certain that this instability would be fully active (Chiang et al. 2002). Therefore, we conclude that these upper limits are not surprising, but they do set constraints on the rather poorly known dispersal mechanisms.

6. SUMMARY AND CONCLUSIONS

One of the goals of the Formation and Evolution of Planetary Systems (FEPS) *Spitzer* Legacy project is to measure the evolution and dispersal of gas in the planet-forming regions (~0.5–40 AU) of disks around solar-type stars of ages 3–100 Myr. We report here our first carefully reduced and analyzed high spectral resolution data, taken by the IRS instrument on *Spitzer*. This paper illustrates our method of modeling the data to obtain constraints on the gas surface density distribution and mass. We eventually plan to obtain data on about 40 nearby stars in this age range to look for variations with age and other stellar properties.

The data presented here are for the source HD 105, a ~30 Myr old G0 star at a distance of 40 pc with a known IR excess arising from a circumstellar dust disk orbiting at $r_{i,\mathrm{dust}} \gtrsim 13$ AU. The derived upper limits to the H_2 $S(0)$ 28 μm, H_2 $S(1)$ 17 μm, H_2 $S(2)$ 12 μm, [S I] 25 μm, [Fe II] 26 μm, and [Si II] 35 μm lines are given in Table 1. The H_2 upper limits directly place limits on the mass of warm gas in the disk: $M(H_2) \lesssim 4.6 M_J$ at 50 K, $3.8 \times 10^{-2} M_J$ at 100 K, and $3.0 \times 10^{-3} M_J$ at 200 K. This can be compared with the roughly $10^{-3} M_J$ of gas detected around β Pic, a 10–20 Myr old A5 star at a distance of about 19 pc (Brandeker et al. 2004). It can also be compared with the recent UV absorption measurements and analysis of AU Mic, an M1 star in the β Pic Moving Group at a distance of 9.9 pc and with a similar age as β Pic (Roberge et al. 2005). They find an upper limit to the H_2 mass of about $2 \times 10^{-4} M_J$. It appears that even in the inner (<30 AU) regions not well probed by CO observations, the gas is largely dissipated in these three sources, which span an age range 10–30 Myr and stellar types from M1 to A5.

Detailed thermal/chemical models of HD 105 were constructed and compared with the *Spitzer* observations to obtain further constraints on the gas mass and surface density. These models calculate the gas temperature, chemistry, and vertical structure self-consistently and predict line fluxes that depend largely on the gas inner radius, $r_{i,\mathrm{gas}}$, and the gas surface density Σ_0 there. We show that most of the gas emission arises in a thin inner rim, extending from $r_{i,\mathrm{gas}}$ to $r_{w,\mathrm{gas}}$, heated by stellar optical, ultraviolet, and X-ray photons. The upper limits on the [S I] 25 μm and [Si II] 35 μm fine-structure lines provide the strongest constraints on the gas surface density Σ_0 at the inner rim.

If the gas inner radius is comparable to the observationally constrained dust inner radius, $r_{i,\mathrm{dust}} \gtrsim 13$ AU, we show that the *Spitzer* upper limits on the line fluxes limit Σ_0 to $\lesssim 0.2$ g cm^{-2} for $r_{i,\mathrm{gas}}$ between 10 and 40 AU. In this case, the total mass of gas (cold and warm) in the planet-forming region between 10 and 40 AU is constrained to be less than $0.1 M_J$ (assuming a constant surface density between $r_{i,\mathrm{gas}}$ and 40 AU).

The gas may not coexist with the dust, however. We show that even if the putative gas extends inward to $r_{i,\mathrm{gas}} = 0.5$ AU, the *Spitzer* upper limits set tight constraints on the gas surface density and mass. The upper limits on the gas surface density are $\Sigma_{0,\mathrm{crit}} = 3.43$, 0.36, and 0.12 g cm^{-2} for $r_{i,\mathrm{gas}} = 0.5$, 1, and 5 AU, respectively. The total mass of gas in the gas giant planet-forming region out to 40 AU depends on how we extrapolate the gas surface density from the inner radius. If we assume a gas surface density power law $\Sigma \propto r^{-3/2}$, which is often assumed in disks, then the total gas mass in these three cases is limited to about 10^{-2}, 3×10^{-3}, and 10^{-2} M_J, respectively. An extreme assumption, allowing for the most hidden cold gas mass, would be a constant surface density with radius. In this case, we obtain total (warm and cold) gas mass limits of 1.9, 0.2, and 0.07 M_J, respectively. In summary, assuming that $r_{i,\mathrm{gas}} > 0.5$ AU and any reasonable gas surface density distribution, there is less than a Jupiter mass of total gas in the gas giant planet forming region out to 40 AU. Given likely temperature distributions produced in our models, *Spitzer* is unlikely to be able to detect *total* gas masses less than about $10^{-2} M_J$ for disks around relatively nearby (~30 pc) low-mass stars.

If the gas extends to $r_{i,\mathrm{gas}} \lesssim 0.5$ AU, the *Spitzer* upper limits set no useful constraints on the gas mass, because gas lines become undetectable even with extremely large gas masses. In this case, the small inner rim that absorbs the heating photons from the star has too little mass (for optically thin lines) and too little surface area (for optically thick lines) to provide detectable *Spitzer* emission, regardless of the magnitude of Σ_0. The outer gas is effectively shielded from the heating photons, and significant cold gas mass could exist in the planet-forming regions. We argue that this

case is unlikely, however, since the gas would likely extend all the way to the stellar surface, and viscous accretion onto the central star would lead to observational diagnostics such as near-infrared or UV excess, Hα emission, and signs of winds generated by the accretion process (which are not observed).

We therefore conclude that the *Spitzer* upper limits imply low upper limits to the gas surface density and mass in the 0.5–40 AU region around HD 105. We also note that, like HD 105, many debris disks will have too little dust to affect the gas spectra; therefore, a similar analysis of *Spitzer* upper limits on line fluxes will result in similar conclusions. As discussed in § 5, the limits are not sufficiently stringent to constrain the potential effects of gas on dust dynamics. They set interesting limits on the mass of gas that might affect terrestrial planet formation only in the ad hoc case in which the inner gas radius is on the order of 0.5–1 AU. However, the limits do set interesting constraints for giant planet formation. The upper limits to the gas mass obtained here are too small to enhance the buildup of gas-poor outer giants such as Uranus or Neptune, and too small to allow for gas giants to form from the gas reservoir after this time ($\sim$30 Myr).

We acknowledge support from NASA's *Spitzer Space Telescope* Legacy program, which has supported our group, the Formation and Evolution of Planetary Systems Legacy team. We thank the rest of the FEPS team for their efforts in making the FEPS project successful, and for their help in obtaining, analyzing, and interpreting the data discussed in this paper.

REFERENCES

Adams, F. C., Hollenbach, D., Laughlin, G., & Gorti, U. 2004, ApJ, 611, 360
Agnor, C. B., & Ward, W. R. 2002, ApJ, 567, 579
Alexander, R. D., Clarke, C. J., & Pringle, J. E. 2005, MNRAS, in press
Balbus, S. A., & Hawley, J. F. 1991, ApJ, 376, 214
Bary, J. S., Weintraub, D. A., & Kastner, J. H. 2003, ApJ, 586, 1136
Beckwith, S. V. W., & Sargent, A. I. 1996, Nature, 383, 139
Blake, G. A., & Boogert, A. C. A. 2004, ApJ, 606, L73
Boss, A. 2003, ApJ, 599, 577
Brandeker, A., Liseau, R., Olofsson, G., & Fridlund, M. 2004, A&A, 413, 681
Brittain, S., et al. 2003, ApJ, 588, 535
Carpenter, J., Wolf, S., Schreyer, K., Launhardt, R., & Henning, T. 2005, AJ, 129, 1049
Carr, J., Mathieu, R., & Najita, J. 2001, ApJ, 551, 454
Chen, C. H., et al. 2004, BAAS, 204, 4106
Chiang, E., Fischer, D., & Thommes, E. 2002, ApJ, 564, L105
Clarke, C. J., Gendrin, A., & Sotomayor, M. 2001, MNRAS, 328, 485
Cutispoto, G., Pastori, L., Pasquini, L., de Medeiros, J., Tagliaferri, G., & Andersen. J. 2002, A&A, 384, 491
Decin, L., Morris, P. W., Appleton, P. N., Charmandaris, V., Armis, L., & Houk, J. R. 2004, ApJS, 154, 408
Dent, W. R. F., Greaves, J. S., & Coulson, I. M. 2005, MNRAS, 359, 663
Dullemond, C. P., & Dominik, C. 2004, A&A, 421, 1075
Dullemond, C. P., Dominik, C., & Natta, A. 2001, ApJ, 560, 957
Dutrey, A., Guilloteau, S., Prato, L., Simon, M., Duvert, G., Schuster, K., & Menard, F. 1998, A&A, 338, L63
Duvert, G., et al. 2000, A&A, 355, 165
Goldreich, P., Lithwick, Y., & Sari, R. 2004, ApJ, 614, 497
Gorti, U., & Hollenbach, D. 2004, ApJ, 613, 424 (GH04)
Greaves, J. S. 2004, MNRAS, 351, L99
Haisch, K. E., Lada, E. A., & Lada, C. J. 2001, ApJ, 553, L153
Henry, T. J., Soderblom, D. R., Donahue, R. A., & Baliunas, S. L. 1996, AJ, 111, 439
Herczeg, G. J., Linsky, J. L., Valenti, J. A., Johns-Krull, C. M., & Wood, B. E. 2002, ApJ, 572, 310
Hillenbrand, L., Strom, S. E., Calvet, N., Merill, M. K., Gatley, I., Makidon, R. B., Meyer, M. R., & Skrutskie, M. F. 1998, AJ, 116, 1816
Hogerheijde, M., Johnstone, D., Matsuyama, I., Jayawardhana, R., & Muzerolle, J. 2003, ApJ, 593, L101
Hollenbach, D. J., Johnstone, D., Lizano, S., & Shu, F. 1994, ApJ, 428, 654
Hollenbach, D. J., Yorke, H. W., & Johnstone, D. 2000, in Protostars and Planets IV, ed. V. Mannings, A. P. Boss, & S. S. Russell (Tucson: Univ. Arizona), 404
Houck, J. R., et al. 2004, ApJS, 154, 18
Houk, N. 1978, Michigan Catalogue of Two-Dimensional Spectral Types for the HD Stars (Ann Arbor: Univ. Michegan)
Hubickyj, O., Bodenheimer, P., & Lissauer, J. J. 2004, RevMexAA Ser. Conf., 22, 83
Johnstone, D., Hollenbach, D. J., & Bally, J. 1998, ApJ, 499, 758
Kessler-Silacci, J. E., Hillenbrand, L. A., Blake, G. A., & Meyer, M. R. 2005, ApJ, 622, 404
Klahr, H. H., & Lin, D. N. C. 2001, ApJ, 554, 1095
Kominami, J., & Ida, S. 2002, Icarus, 157, 43
———. 2004, Icarus, 167, 231
Kornet, K., Bodenheimer, P., & Rozyczka, M. 2002, A&A, 396, 977
Lecavalier des Etangs, A., et al. 2001, Nature, 412, 706
Levison, H. F., & Stewart, G. R. 2001, Icarus, 153, 224
Lissauer, J. 1993, ARA&A, 31, 129
Mamajek, E., Meyer, M., Hinz, P., Hoffmann, W., Cohen, M., & Hora, J. 2004, ApJ, 612, 496
Matsuyama, I., Johnstone, D., & Hartmann, L. 2003, ApJ, 582, 893
Metanomski, A. D. F., Pasquini, L., Krautter, J., Cutispoto, G., & Fleming, T. A. 1998, A&AS, 131, 197
Meyer, M. R., et al. 2004, ApJS, 154, 422 (M04)
Miyake, K., & Nakagawa, Y. 1993, Icarus, 106, 20
Najita, J., Carr, J., & Matheiu, R. 2003, ApJ, 589, 931
Natta, A., Testi, L., Neri, R., Shepherd, D., & Wilner, D. 2004, A&A, 416, 179
Perryman, M. A. C., et al. 1997, A&A, 323, L49
Pietu, V., Dutrey, A., & Kahane, C. 2003, A&A, 398, 565
Pollack, J., Hubickyj, O., & Bodenheimer, P. 1996, Icarus, 124, 62
Przygodda, F., et al. 2003, A&A, 412, L43
Qi, C., Kessler, J. E., Koerner, D. W., Sargent, A. I., & Blake, G. A. 2003, ApJ, 597, 986
Randich, S., Pallavicini, R., Meola, G., Stauffer, J., & Balachandran. S. 2001, A&A, 373, 862
Rettig, T. W., Haywood, J., Simon, T., Brittain, S. D., & Gibb, E. 2004, ApJ, 616, L163
Richter, M., Jaffe, D. T., Blake, G. A., & Lacy, J. H. 2002, ApJ, 572, 161
Roberge, A., Weinberger, A. J., Redfield, S., & Feldman, P. D. 2005, ApJ, 626, L105
Sako, S., et al. 2005, ApJ, 620, 347
Sheret, I., Ramsey Howat, S. K., & Dent, W. R. F. 2003, MNRAS, 343, L65
Silverstone, M. 2000, Ph.D. thesis, Univ. California, Los Angeles
Skrutskie, M. F., Snell, R., Dutkevitch, D., Strom, S. E., Schloerb, F. P., & Dickman, R. L. 1991, AJ, 102, 1749
Soderblom, D. R., Oey, M. S., Johnson, D. R. H., & Stone, R. P. S. 1990, AJ, 99, 595
Suttner, G., & Yorke, H. W. 2001, ApJ, 551, 461
Takeuchi, T., & Artymowicz, P. 2001, ApJ, 557, 990
Takeuchi, T., & Lin, D. N. C. 2002, ApJ, 581, 1344
Testi, L., Natta, A., Shepherd, D. S., & Wilner, D. J. 2003, A&A, 403, 323
Thebault, P., & Augereau, J.-C. 2005, A&A, 437, 141
Thi, W.-F., van Dalen, B., Bik, A., & Waters, L. B. F. M. 2005, A&A, 430, L61
Thi, W. F., et al. 2001, ApJ, 561, 1074
Throop, H. B., Bally, J., Esposito, L. W., & McCaughrean, M. J. 2001, Science, 292, 1686
van Boekel, R., Waters, L. B. F. M., Dominik, C., Bouwman, J., de Kotter, A., Dullemond, C. P., & Paresce, F. 2003, A&A, 400, L21
van Dishoeck, E. F. 2004, ARA&A, 42, 119
Weidenschilling, S. J. 1977, MNRAS, 180, 57
Weidenschilling, S. J., et al. 1997, Icarus, 128, 429
Weinberger, A., Becklin, E., Zuckerman, B., & Song, I. 2004, AJ, 127, 2246
Werner, J. R., et al. 2004, ApJS, 154, 1
Wolf, S., & Hillenbrand, L. A. 2003, ApJ, 596, 603
Wolf, S., Padgett, D., & Stapelfeldt, K. R. 2003, ApJ, 588, 373
Wichmann, R., Schmitt, J., & Hubrig, S. 2003, A&A, 399, 983
Zuckerman, B., Forveille, T., & Kastner, J. H. 1995, Nature, 373, 494